# Fluidically Reconfigurable MIMO Antenna With Pattern Diversity for Sub-6-GHz 5G Relay Node Applications

# Antenne EMSM reconfigurable fluidique avec diversité de motifs pour les applications de noeuds de relais 5G sous-6 GHz

Aditya Singh and Carlos E. Saavedra, *Senior Member, IEEE*

***Abstract*—A four-element frequency reconfigurable and pattern diverse multiple-input–multiple-output (MIMO) antenna array for fifth-generation relay node applications is presented to operate in LTE bands 42 (3400–3600 MHz), 43 (3600–3800 MHz), and 46 (5150–5925 MHz). A planar microstrip line-fed monopole antenna is utilized as the MIMO element. The antenna relies on fluidic reconfiguration mechanism to either serve LTE bands 42/43 or 46. It incorporates a substrate milled channel beneath each monopole arm to hold distilled water. The water in the channel perturbs the *E*-field distribution in the vicinity of the antenna arm and modifies the effective permittivity of the dielectric medium. To realize pattern diversity, adjacent elements are placed orthogonal to each other. Measured prototype exhibits a total active reflection coefficient |TARC| and $|S_{11}| \leq -10$ dB for the high band when the channel is vacant (case 1) and the low band when filled with water (case 2), while minimum isolation is above 19.6 dB. The peak measured gain is ∼4.6 and ∼2.8 dBi, while the worst case envelope correlation coefficient (ECC) is ∼0.004 and ∼0.016 for cases 1 and 2, respectively. It measures 82.4 × 82.4 mm$^2$ and was fabricated on a 1.52-mm-thick substrate of $\epsilon_r = 3.55$.**

***Résumé*—Un réseau d'antennes entrées multiples et sorties multiples (EMSM) à fréquence reconfigurable à quatre éléments et de diversité à motifs pour les applications de noeud de relais de cinquième génération est présenté pour fonctionner dans les bandes ELT 42 (3400–3600 MHz), 43 (3600–3800 MHz) et 46 (5150–5925 MHz). Une antenne unipolaire alimentée par ligne microruban plane est utilisée comme élément EMSM. L'antenne repose sur un mécanisme de reconfiguration fluidique pour desservir les bandes ELT 42/43 ou 46. Elle comprend un substrat de canal moulu sous chaque bras monopolaire pour contenir de l'eau distillée. L'eau dans le canal perturbe la distribution du champ E au voisinage du bras d'antenne et modifie la permittivité effective du milieu diélectrique. Pour réaliser la diversité de motifs, les éléments adjacents sont placés orthogonalement les uns aux autres. Le prototype mesuré présente un coefficient de réflexion actif total |TARC| et $|S_{11}| \leq -10$ dB pour la bande haute lorsque le canal est vacant (cas 1) et la bande basse lorsque remplie d'eau (cas 2), alors que l'isolation minimale est supérieure à 19,6 dB. Le gain maximal mesuré est d'environ 4,6 et de 2,8 dBi, tandis que le coefficient de corrélation d'enveloppe (ECC) dans le pire des cas est respectivement de 0,004 et 0,016 pour les cas 1 et 2. Il mesure 82,4 × 82,4 mm$^2$ et a été fabriqué sur un substrat de 1,52 mm d'épaisseur de $\epsilon_r = 3{,}55$.**

***Index Terms*—Antennas, dielectric fluid, distilled water, envelope correlation coefficient (ECC), fifth generation (5G), fluidic, high power, microfluidics, monopole, multiple-input multiple-output (MIMO), pattern diversity, reconfigurable.**

## I. Introduction

THE fifth-generation (5G) wireless network architecture is a heterogeneous multitier system encompassing a coverage tier and a hotspot tier [1], [2]. The coverage tier provides high capacity, reliable, and wide coverage links, while the hotspot tier is dedicated to high data-rate, short-range, and primarily indoor links [2]. For the 5G Coverage tier, the 3400–3800-MHz frequency band comprising of long-term evolution (LTE) bands 42 and 43 has been allocated [3]. Moreover, to allocate more bandwidth, the LTE license assisted access (LTE–LAA) band (5150–5925 MHz) is also provided in the sub-6-GHz regime. 5G will utilize the multiple-input–multiple-output (MIMO) antenna technology to obtain the best data rate for a given frequency bandwidth and allowable power levels [4]. MIMO antennas perform the best when they fully utilize a rich scattering environment. However, if MIMO antennas with pattern diversity are employed, they show good performance even in poor scattering environments [5].

Manuscript received April 23, 2019; revised September 25, 2019; accepted October 24, 2019. Date of current version January 28, 2020. This work was supported in part by the Natural Sciences and Engineering Research Council of Canada (NSERC) under Grant STPGP-521223-2018. *(Corresponding author: Aditya Singh.)*

The authors are with the Department of Electrical and Computer Engineering, Queen's University, Kingston, ON K7L 3N6, Canada (e-mail: aditya.singh@queensu.ca).

Associate Editor managing this article's review: Ahmed Refaey Hussein.
Digital Object Identifier 10.1109/CJECE.2019.2950133

Many studies reveal that in the coverage tier, MIMO antennas in the relay nodes are anticipated to play an important role in 5G to provide extended coverage at cell edges as well as for indoor applications [6]–[9]. These nodes can provide enhanced throughput by employing nonorthogonal multiple access (NOMA) with increased relay power capacity [10]. Furthermore, such nodes need to be low profile and wall mountable. Thus, to obtain the best performance from the 5G relay nodes in LTE 42, 43, and 46 bands, planar, pattern diverse, and frequency reconfigurable MIMO antennas with high-power handling are highly suitable.

Recently, in the field of reconfigurable antenna, the fluidic mechanism for reconfiguration due to their liquid nature has attracted a lot of attention to overcome limited reliability of mechanically triggered counterparts. Easy movement of fluid eradicates issues arising from the movement of solid parts that cause fatigue, wear, and tear [11]. Notably, the linear nature of switching element in fluidic reconfigurations enables antennas to maintain linearity in applications involving high average power. However, switching speeds are slower compared with semiconductor devices. The choices for the fluids are vast and depend on the type of application. In RF design, liquid metals have extensively been sought in design of various antennas with reconfigurable radiation pattern [11], polarization [12]–[14], and filters [15], [16]. Liquid metal-based designs face issues in integration with the antenna structure, and the residues of oxidized liquid metal in the fluidic channel are difficult to handle. Thus, even after using micropumps for automated pressurized actuations, liquid metal-based techniques remain arduous to design. To circumvent these problems, various techniques have been proposed [17], [18].

Liquid dielectric-based methods are not severely affected and present a viable alternative. Moreover, the conductivity of the liquid dielectric is usually very low, and hence, new methods for reconfiguration need to be investigated. Different types of fluids have been adopted in high-frequency design, such as ethyl alcohol [19], [20], acetone [21], transformer oil [22], and water [19], [21], [23]–[29]. In [21], a microstrip patch antenna with two microchannels integrated under the radiating edges is reported. A wide frequency tuning range is achieved with injection of dielectric liquids, such as water, acetone, methanol, and ethanol. However, the radiation efficiency is only 27%. In [23], a water-filled dielectric resonator antenna, fed with a probe, is realized on a glass container having multiple layers. For frequency tuning, the height of the antenna is varied through successive loading of the layers with water. This nonplanar design is shown to exhibit frequency tuning of 52% with respect to the center frequency. Water has also been employed to provide radiation pattern reconfiguration [27], [28] and polarization reconfiguration, as in [30]. In the antenna array regime, few fluidics-based antennas have been reported. For instance, two-element water-based MIMO antenna in [24] offers good bandwidth and efficiency but with degraded ECC performance. Reference [25] implements a 2 × 2 antenna array using aperture-coupled water dielectric patch antenna exhibiting good gain but lacks reconfigurability. Qian and Chu [31] present the two-element water loaded pattern reconfigurable MIMO antenna with good ECC and gain but only with 11% impedance bandwidth (IBW).

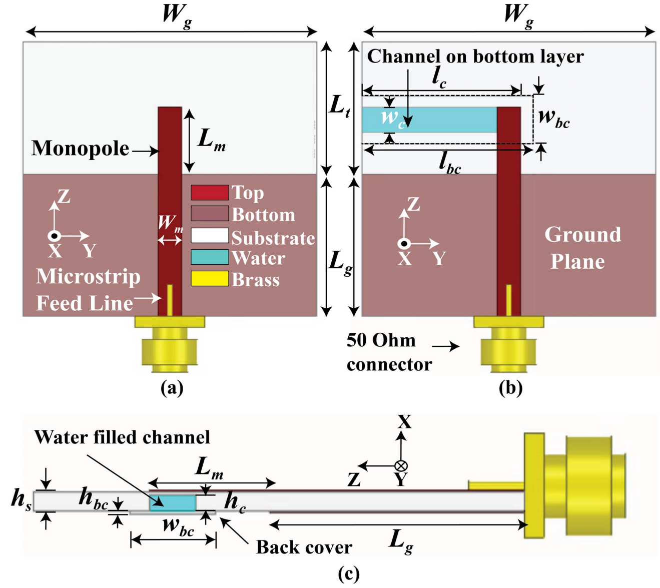


Fig. 1. Reference and reconfigurable monopole antenna (RMA) model: $L_g = 25$, $L_t = 20$, $L_m = 11$, $W_g = 40$, $W_m = 3.3$, $h_{bc} = 0.2$, $w_{bc} = 7.35$, $l_{bc} = 23.3$, $h_c = 1.24$, $l_c = 21.65$, $w_c = 4.2$, and $h_s = 1.52$ (all dimensions in this article are in mm). (a) Reference monopole antenna. (b) RMA element. (c) Cross section of the RMA showing water-filled channel.

In this article, a four-element frequency reconfigurable and pattern diverse MIMO array is presented. A reconfigurable low-profile microstrip line-fed monopole is utilized as the MIMO element. We first discuss the design for reconfigurable single element operating in LTE bands 42 and 43 or 46 and follow-up with a four-element MIMO array. The element orientation in the antenna aids to provide pattern diversity and, hence, lower ECC to ensure good MIMO performance with reasonable antenna efficiency over all the frequency bands of interest.

## II. Reconfigurable MIMO Element Design

The monopole in [32] is redesigned on a 1.52-mm-thick Rogers 4003 substrate ($\epsilon_r = 3.38$, $\tan\delta = 0.0027$), as shown in Fig. 1(a), to yield 40% −10-dB IBW with the fixed center frequency of around 5 GHz. The ground plane size is tuned in ANSYS HFSS electromagnetic (EM) simulations to obtain a large IBW of 1.9 GHz, while the monopole width is tuned for best impedance match of ∼−26 dB. This reference antenna, however, can only serve the LTE band 46 with the single-band operation. Therefore, to enable antenna operation on LTE band 42/43 as well as LTE band 46, a fluidic reconfiguration mechanism is incorporated by partially milling out the substrate beneath the monopole arm open end, as shown in Fig. 1(b), to create a channel, as described in [32] and [33]. The four element MIMO antenna using this element is shown in Fig. 2.

To switch operation to lower bands, the created channel is filled with distilled water. The high relative permittivity of distilled water introduces discontinuities in the modified medium. Water-filled channels perturb the $E$-field distribution around the monopole arm altering the input impedance of the

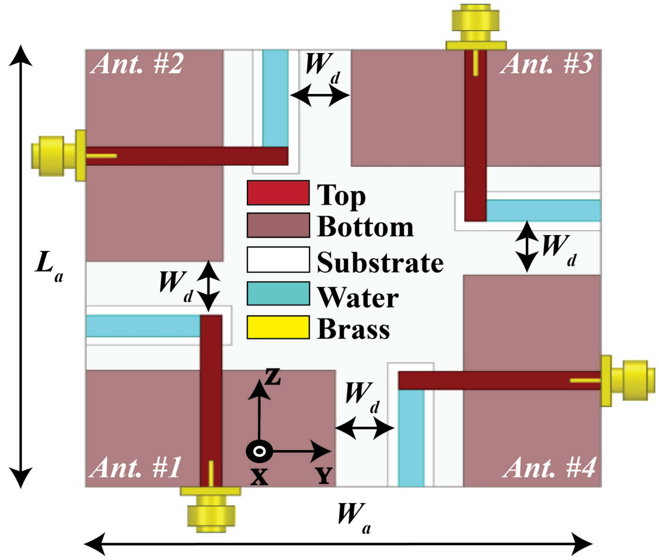


Fig. 2. Proposed four-element MIMO RMA array is shown where each antenna channel is filled with water: $L_a = 82.4$, $W_a = 82.4$, and $W_d = 10$ (rest of the design parameters are same as the RMA element shown in Fig. 1).

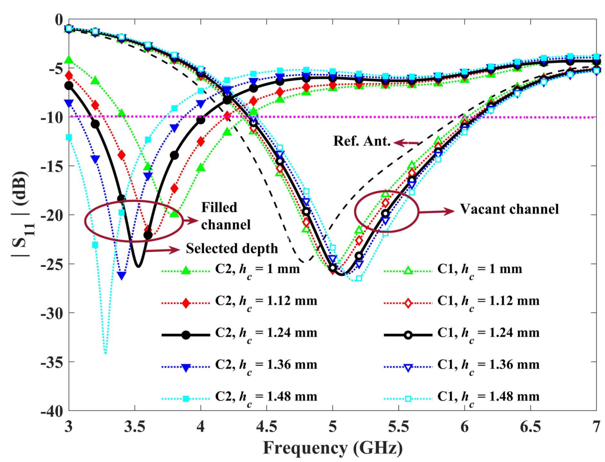


Fig. 3. Simulated curves of | $S_{11}$ | for the RMA element shown in Fig. 1(b) with variation in channel depth. C1: vacant (air filled) channel case. C2: water-filled channel case.

antenna. In effect, the effective dielectric permittivity seen by the excited waves inside the structure increases. Thus, for the monopole antenna, the $\lambda_g/4$ (where $\lambda_g$ is guided wavelength in microstrip environment [34]) resonance shifts to a lower frequency, as shown in Fig. 3. The dielectric constant and loss tangent for distilled water are modeled in EM simulations using the experimentally verified data at 20 °C ($\epsilon_r \sim 76.9$ and $\tan\delta \sim 0.2$ at 3.6 GHz) from [35]. As intuitively evident, for the water-filled case, more volume of water in proximity to monopole arm results in larger frequency shift; however, the bandwidth tends to reduce, as reported in [32] and [33]. To accommodate this effect, the antenna is designed with large IBW for vacant channel case. Subsequently, the depth of the water channel is varied to select the depth that offers the required bandwidth of at least 400 MHz around 3.6 GHz. Fig. 3 depicts the variation of | $S_{11}$ | as the channel depth changes from 1 to 1.48 mm for the antenna shown in Fig. 1(b). As seen, for the air-filled

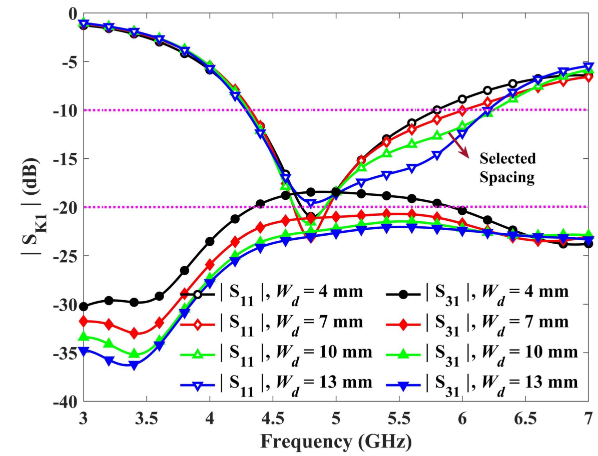


Fig. 4. Simulated variation of | $S_{K1}$ | ($K = 1$ and 3) for RMA array shown in Fig. 2 with tuning of interelement spacing (only | $S_{31}$ | shown, | $S_{21}$ | and | $S_{41}$ | are identical and have lower | $S_{K1}$ | values).

channel case (C1), the resonant frequency changes slightly by ~3.5%, while for water-filled case (C2), resonant frequency shows a larger change of ~13.5%. Furthermore, the channel depth of 1.24 mm is selected, as it provides the required IBW and impedance match to cover LTE bands 42 and 43 (3400–3800 MHz) when filled with water (case C2) and LTE band 46 (5.15–5.925 GHz) when vacant (case C1).

## III. Reconfigurable MIMO Antenna Array

### A. Reflection and Isolation Characteristics

Fig. 2 shows the model of the proposed MIMO antenna with all the design parameters. In this MIMO array, four elements are used, and they are arranged such that adjacent monopole elements are orthogonal to each other. It also implies that the diagonally opposite elements are placed in opposite directions, as in [36]. Consequently, the mutual coupling between the elements is reduced, and exciting different ports results in radiation pattern diversity as the relative position of the other elements changes when different elements are excited. Furthermore, four ports are provided to excite the respective antenna element. The interelement spacing in this scenario is crucial as it impacts both IBW and the isolation between the MIMO elements. The isolation between the antenna elements is critical to obtain good MIMO performance. The higher isolation results in decoupled antenna elements leading to improved envelope correlation coefficient (ECC). Fig. 4 shows | $S_{11}$ | and | $S_{31}$ | curves to understand the IBW and isolation performance. The | $S_{21}$ | and | $S_{41}$ | curves have lower values, so they have been omitted from Fig. 4 for sake of clarity. As the spacing $W_d$ is increased from 4 to 10 mm, the IBW improves from 1.48 to 1.9 GHz, while the minimum isolation changes from 18.4 to 22.5 since the EM coupling decreases as the spacing between the elements increases. It is evident that $W_d = 10$ mm keeps the size acceptable for relay node-based applications and maintains the required IBW and isolation better than 20 dB for all the ports. The reflection and isolation for the antenna is reported in Figs. 5 and 6 for vacant and water filled channels, respectively. It should be noted that since the antenna is symmetric with respect to

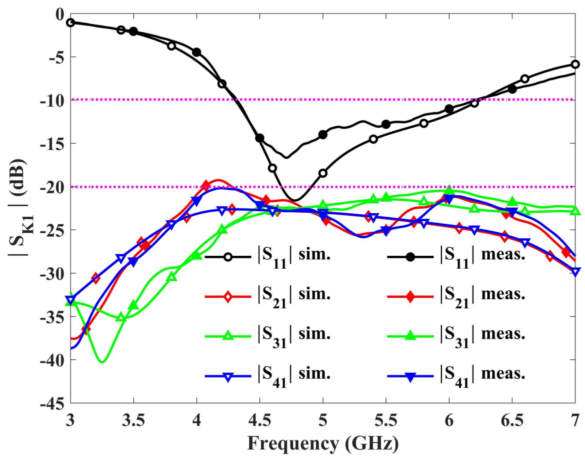


Fig. 5. Simulated and measured | $S_{K1}$ | ($K$ = 1, 2, 3, and 4) for RMA array with all the channels vacant (filled with air). Results are shown for port 1 excitation with the rest of the ports being terminated with 50 Ω.

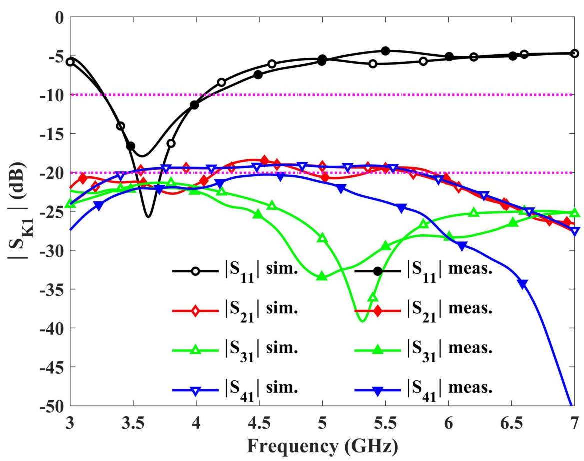


Fig. 6. Simulated and measured | $S_{K1}$ | ($K$ = 1, 2, 3 and 4) for RMA array with all the channels filled with water. Results are shown for port 1 excitation with the rest of the ports being terminated with 50 Ω.

each port, the S-parameters' results are the same irrespective of which port is excited keeping other ports terminated. Therefore, S-parameters for the case where port 1 is excited and other ports are terminated with 50 Ω are provided in this article, while other cases are assumed to be identical. In addition, the magnitude of the surface current distribution depicted in Fig. 7 clearly shows the low mutual coupling between the antenna elements. This is evident from the fact that very low surface currents are excited on other elements when port 1 is excited. Relatively, the higher coupling between elements 1 and 4 is observed when the channel is filled with water, as shown in Fig. 7(b). As a result, lower isolation is achieved in this case (| $S_{41}$ | degrades by ~2 dB). The prototype of the antenna is fabricated, as shown in Fig. 8, using the in-house LPKF circuit plotter to corroborate the simulated results. In Fig. 5, showing results for the vacant channel, the simulated and measured responses show reasonable agreement. The measured IBW is ~ 1.9 GHz, while the worst case isolation in the LTE band 46 is ~ −21 dB. In the next step, the channel is filled with distilled water from the inlet port using a syringe. The | $S_{11}$ | response

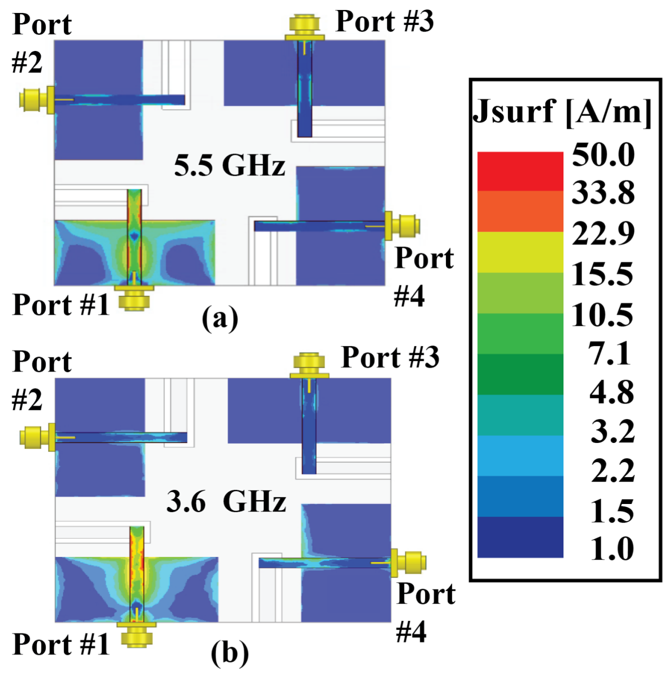


Fig. 7. Surface electric current distribution on antenna when port 1 is excited and rest of ports are terminated with 50 Ω. (a) Vacant (air-filled) channels (5.5 GHz). (b) Water-filled channels (3.6 GHz).

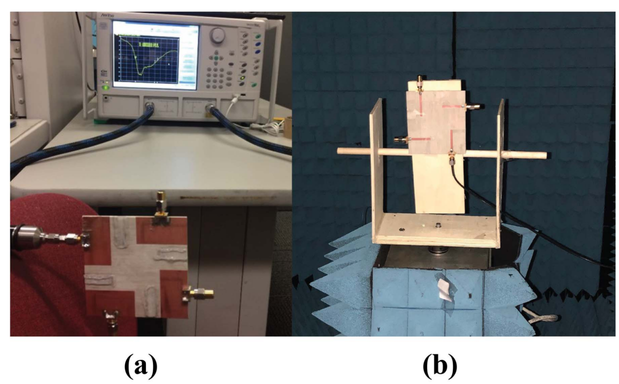


Fig. 8. Prototype of proposed four-element MIMO antenna array. (a) Back view of an antenna in the S-parameter measurement setup with a vector network analyzer (VNA). (b) Front view of the antenna with the radiation measurement setup in an anechoic chamber.

shifts downward, as shown in Fig. 6 with impedance match of −25 dB and spanning measured IBW of 0.8 GHz, which is sufficient to cover both LTE bands 42 and 43. The RF connector model is incorporated in the simulation results to minimize the differences in impedance matching and bandwidth for the measured results compared to simulations. However, observed differences can be attributed to fabrication tolerances, mismatches caused by the glue, and possible discrepancies in modeling distilled water dielectric constant and loss tangent.

### B. Far-Field and MIMO Response

The far-field response of the antenna is analyzed by exciting one port at a time and terminating rest of the ports with 50 Ω. The far-field response for the air-filled channel is first discussed. To emphasize the radiation pattern diversity of the proposed antenna, the 3-D gain pattern is presented

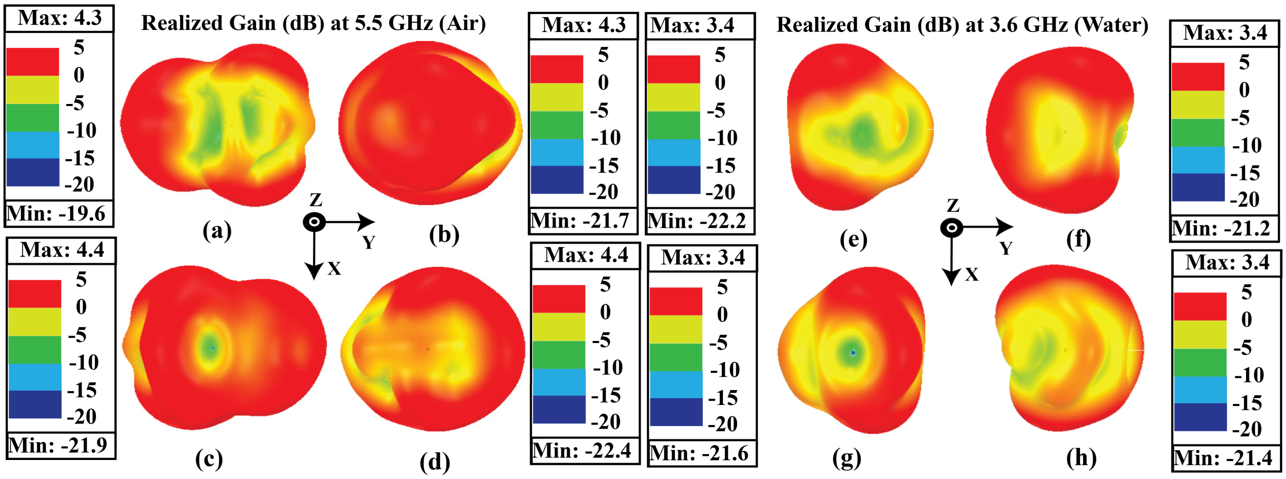


Fig. 9. 3-D realized gain (dBi) of the antenna when one port is excited and rest of ports are terminated to 50 Ω. (a) Port 1, (b) Port 2, (c) Port 3, and (d) Port 4 for channels filled with air (5.5 GHz). (e) Port 1, (f) Port 2, (g) Port 3, and (h) Port 4 for channels filled with water (3.6 GHz).

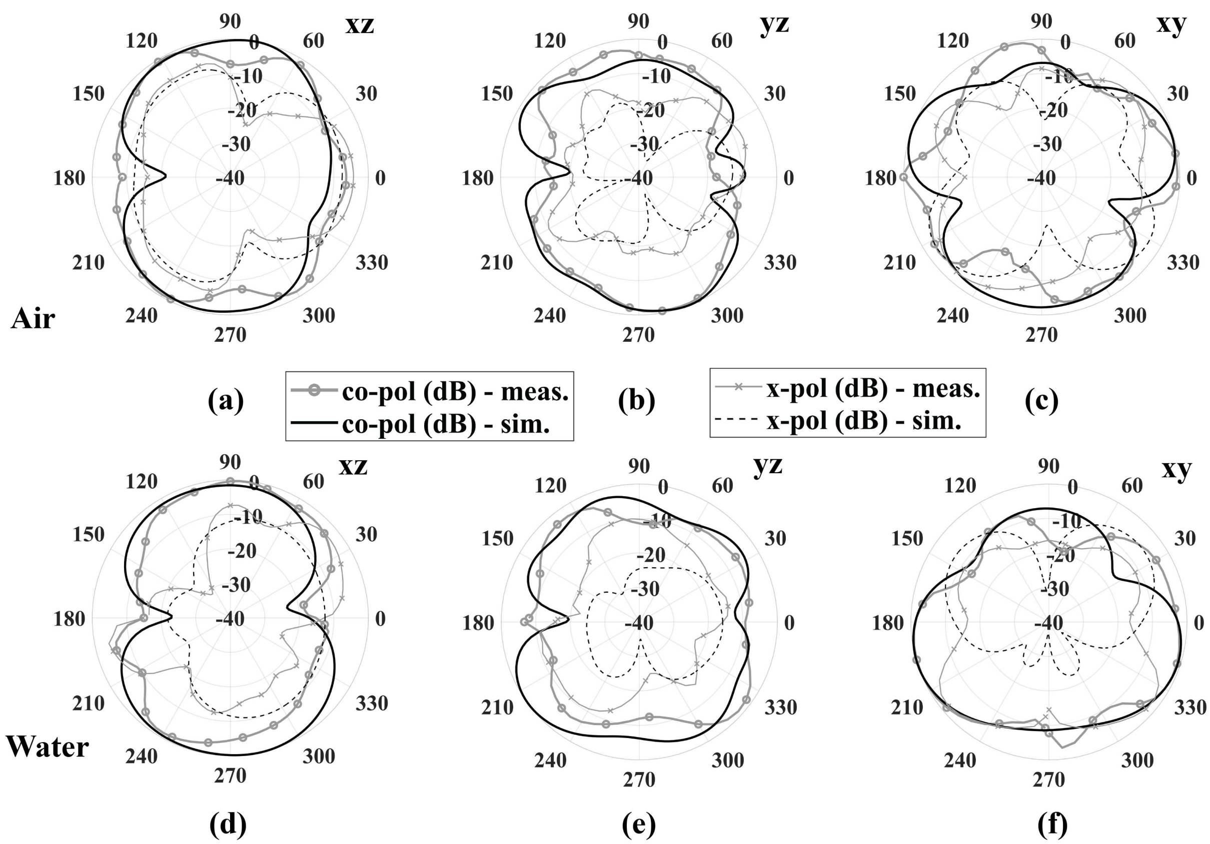


Fig. 10. Normalized radiation pattern of the antenna when port 1 is excited and rest of ports are terminated to 50 Ω. (a) $xz$ plane, (b) $yz$ plane, and (c) $xy$ plane for channels filled with air (5.5 GHz). (d) $xz$ plane, (e) $yz$ plane, and (f) $xy$ plane for channels filled with water (3.6 GHz).

in Fig. 9. When port 1 is excited, the gain pattern resembles that of a $z$-directed monopole but modified due to presence of other elements in the vicinity. In this case, element 4 acts as a reflector for fields radiated in the $+y$-direction and, thus, consolidates radiation toward opposite $(-y)$ direction. However, element 2 shows minimal impact on the pattern as it is placed along the null direction and similar reasoning follows for element 3 as it is located farther away.

Consequently, element 1 excitation exhibits a monopole-like pattern with dominant radiation along the $+x$-, $-x$-, and $-y$-directions with nulls along the $z$-axis. To further corroborate this line of reasoning, it can be observed in Fig. 7(a) that currents in element 4 have higher magnitude compared to elements 2 and 3. Hence, element 4 shows the dominant impact on radiation pattern when port 1 is excited. The simulated maximum gain observed is 4.3 dBi at 5.5 GHz. Notably, the 3-D pattern for element 3 excitation is a mirror image of the element 1 case. This is quite obvious as in this case, fields are reflected in the $+y$-direction dominantly by element 2. However, port 2 excitation shows even more diverse radiation pattern enabling radiation along the $z$-axis. Again, the pattern is monopole-like with major radiation

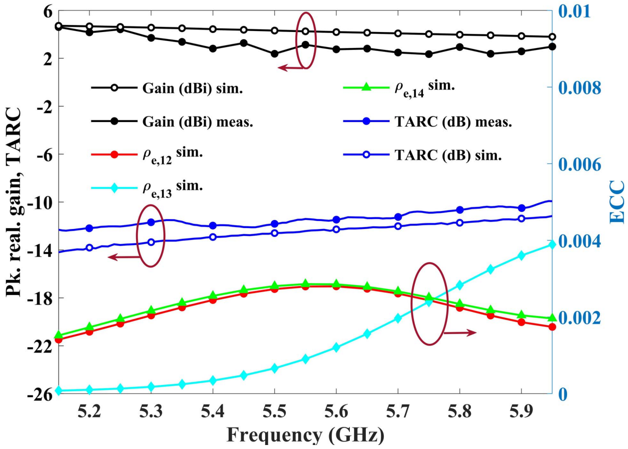


Fig. 11. Measured realized gain (dBi), TARC (dB), and the simulated ECC for vacant channel case in LTE band 46 when port1 is excited and the rest of ports terminated with 50 Ω.

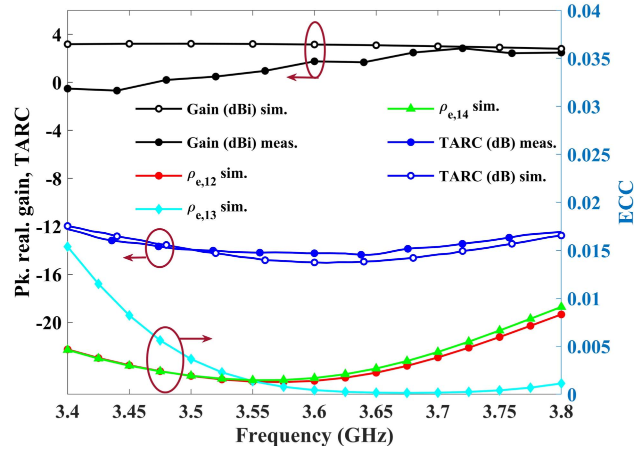


Fig. 12. Measured realized gain (dBi), TARC (dB), and the simulated ECC for water-filled channel case in LTE bands 42 and 43 when port1 is excited and rest of ports terminated with 50 Ω.

in the $+x$-, $-x$-, and $+z$-directions due to similar reasons cited for port 1 case. However, this time element 1 acts as an effective reflector. The maximum simulated gain is again 4.3 dBi. For reasons mentioned earlier, element 4 excitation exhibits mirrored pattern with main radiation in the $+x$-, $-x$-, and $-z$-directions. For the second case, similar pattern diversity is observed when different ports are excited. However, due to the effect of the discontinuity created by the water in the channel, patterns are different compared with the first case. When port 1 is excited, the 3-D radiation pattern is monopole-like with the $+x$, $-x$, and $-z$ dominant directions of radiation. While port 3 pattern remains mirrored compared to port 1 results, port 2 excitation results in a similar pattern and main directions as $+x$, $-x$ and $+y$, while port 4 results being a mirror image of port 2 case, as shown in Fig. 9. Since the frequency of operation is lowered, the relative size of the elements becomes smaller as compared to the guided wavelength, and consequently, the gain reduces. Compared to the air-filled channels, where the adjacent reflecting element has a dominant effect, here, water in the channel exhibits dominance in redirecting the radiation along the null directions of the monopoles, as reported in [32].

The radiation pattern and gain for the prototype antenna are measured in the anechoic chamber to evaluate the practical performance. The measurements are carried out for principal cut planes. Since all the elements are same, measurements are presented for the case when element 1 is excited and the rest of ports are terminated. Similar performance is expected for other ports. In Fig. 10, acceptable agreement between the simulated and measured patterns is observed for both the cases when channels are filled with air and water, respectively. Furthermore, the maximum measured realized gain for case 1 is around 4.6 dBi, as shown in Fig. 11, while for case 2, it is 2.8 dBi, as shown in Fig. 12. The total active reflection coefficient (TARC) is essential to evaluate the effect of mutual coupling and random signal combinations among elements in MIMO antennas and is defined as [4]

$$\text{TARC (dB)} = 10 \log \frac{\sum_{i=1}^{4} \mid b_i \mid^2}{\sum_{i=1}^{4} \mid a_i \mid^2} \tag{1}$$

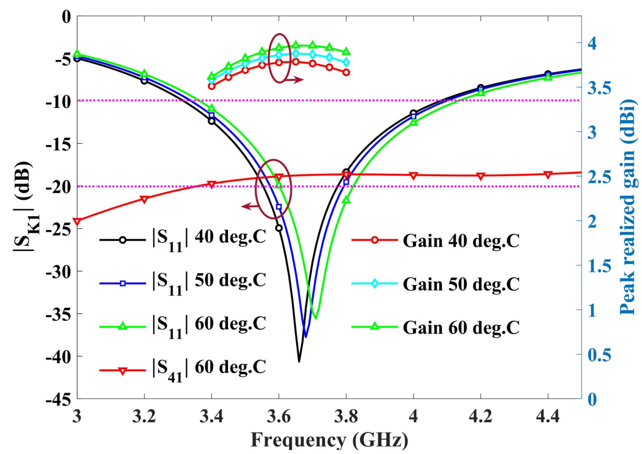


Fig. 13. Simulated $S$-parameters and gain with temperature as the input power increases (60 °C for 15-W input power [37]). Results are plotted when port1 is excited and the rest of ports are terminated with 50 Ω.

where $a_i$ and $b_i$ are incident and reflected signals at the $ith$ port. For both low- and high-band operations, TARC $< -10$ dB is achieved for both simulated and measured results. Furthermore, the simulated ECC is calculated from simulated far fields in HFSS. As shown in Figs. 11 and 12, the ECC ($\rho_e$) remains considerably low to get good MIMO performance over the bands of interest. To ascertain the high-power handling capability, the behavior of antenna at higher surface temperatures due to heating may be evaluated. It is known that the temperature on microstrip antennas can reach up to 60 °C for high input power (15 W) [37]. Using the dielectric properties of water at different temperatures from [35], Fig. 13 shows the stable performance of the simulated IBW, input match, worst case isolation, and gain performance, as the temperature of the antenna increases up to 60 °C. Finally, the minimum simulated total efficiency for case 1 is 90%, while for case 2, it is 76%. Table I shows a performance comparison between the proposed antenna and other fluidic-based arrays.

TABLE I
COMPARISON WITH THE REPORTED WATER-BASED MIMO ANTENNAS

| Ref. | Size (mm$^2$) | IBW (MHz) | Sim. effi (%) | Sim. ECC | Reconfigurable? | MIMO order | Min. Iso. (dB) | Max. Meas. Gain (dBi) |
|---|---|---|---|---|---|---|---|---|
| [24] | 40 × 70 | 2400 - 3340 | $\leq$ 0.60 | $\leq$ 0.36 | no | (2 × 1) | $\geq$ 13 | - |
| [31] | 200 × 200 | 880 - 980 | 80-90 | $\leq$ 0.0001 | yes | (2 × 1) | $\geq$ 35 | 13 |
| This* | 82.4 × 82.4 | 3400 - 3800 (LB) | 76 - 78 | $\leq$ 0.016 | yes | (4 × 4) | $\geq$ 19.6 | 2.8 |
| This* | 82.4 × 82.4 | 5150 - 5925 (HB) | 90 - 96 | $\leq$ 0.004 | yes | (4 × 4) | $\geq$ 20 | 4.6 |

* This work shows -10 dB IBW of 800 MHz in LB (3260 - 4060 MHz) and 1940 MHz in HB (4290 - 6230 MHz) . However, far field results and MIMO metrics have been presented only for LTE band 42/43 and 46.

## IV. CONCLUSION

A four-element frequency reconfigurable MIMO antenna has been reported. A simple planar and low-profile microstrip line-fed monopole antenna has been utilized as the MIMO element. The liquid dielectric loading-based reconfigurable mechanism has been employed through easy integration of the fluidic channel beneath the monopole arm. The channel has been realized by partially milling out the substrate through LPKF circuit plotter and attaching a thin substrate to the backside of the substrate. The parameters for the antenna ground plane and channel cross section were optimized to extract the best input reflection characteristics, gain, and efficiency to cover the LTE band 46 for vacant channel case and LTE bands 42 and 43 for the fluidically switched case. To switch to lower bands, the channel is filled with water, and simultaneous simulations were carried out to meet the requirements in these low bands while maintaining performance in the high band 46. Furthermore, in the proposed MIMO antenna, adjacent elements are placed orthogonal to each other; thus, the antenna exhibits radiation pattern diversity and frequency reconfigurability to operate in LTE bands 42, 43, and 46. A prototype of the proposed design was fabricated and measured showing good agreement with the simulated results. Furthermore, to evaluate the high input power operation and, hence, higher operating temperatures, the antenna has been simulated at elevated temperatures of 40 °C, 50 °C, and 60 °C, showing stable performance.

## ACKNOWLEDGMENT

The authors would like to thank I. Goode for helpful discussions regarding radiation measurements.

## REFERENCES

[1] J. G. Andrews *et al.*, "What will 5G be?" *IEEE J. Sel. Areas Commun.*, vol. 32, no. 6, pp. 1065–1082, Jun. 2014.

[2] E. Björnson, J. Hoydis, and L. Sanguinetti, "Massive MIMO networks: Spectral, energy, and hardware efficiency," *Found. Trends Signal Process.*, vol. 11, nos. 3–4, pp. 154–655, 2017.

[3] WRC Press Release. (Nov. 27, 2015). *World Radiocommunication Conference Allocates Spectrum for Future Innovation*. [Online]. Available: http://www.itu.int/net/pressoffice/pressr_releases/2015/56.aspx

[4] M. S. Sharawi, "Printed multi-band MIMO antenna systems and their performance metrics [wireless corner]," *IEEE Antennas Propag. Mag.*, vol. 55, no. 5, pp. 218–232, Oct. 2013.

[5] M. D. Migliore, D. Pinchera, and F. Schettino, "Improving channel capacity using adaptive MIMO antennas," *IEEE Trans. Antennas Propag.*, vol. 54, no. 11, pp. 3481–3489, Nov. 2006.

[6] Y. Wu, L. P. Qian, H. Mao, X. Yang, H. Zhou, and X. S. Shen, "Optimal power allocation and scheduling for non-orthogonal multiple access relay-assisted networks," *IEEE Trans. Mobile Comput.*, vol. 17, no. 11, pp. 2591–2606, Nov. 2018.

[7] L. Dai, B. Wang, Y. Yuan, S. Han, C.-L. I, and Z. Wang, "Non-orthogonal multiple access for 5G: Solutions, challenges, opportunities, and future research trends," *IEEE Commun. Mag.*, vol. 53, no. 9, pp. 74–81, Sep. 2015.

[8] Z. Ding *et al.*, "Application of non-orthogonal multiple access in LTE and 5G networks," Nov. 2015, *arXiv:1511.08610*. [Online]. Available: https://arxiv.org/abs/1511.08610

[9] Z. Ding, X. Lei, G. K. Karagiannidis, R. Schober, J. Yuan, and V. Bhargava, "A survey on non-orthogonal multiple access for 5G networks: Research challenges and future trends," Jun. 2017, *arXiv:1706.05347*. [Online]. Available: https://arxiv.org/abs/1706.05347

[10] X. Liu, X. Wang, and Y. Liu, "Power allocation and performance analysis of the collaborative NOMA assisted relaying systems in 5G," *China Commun.*, vol. 14, no. 1, pp. 50–60, Jan. 2017.

[11] D. Rodrigo, L. Jofre, and B. A. Cetiner, "Circular beam-steering reconfigurable antenna with liquid metal parasitics," *IEEE Trans. Antennas Propag.*, vol. 60, no. 4, pp. 1796–1802, Apr. 2012.

[12] A. H. Naqvi and S. Lim, "Microfluidically polarization-switchable metasurfaced antenna," *IEEE Antennas Wireless Propag. Lett.*, vol. 17, no. 12, pp. 2255–2259, Dec. 2018.

[13] M. Wang, M. R. Khan, M. D. Dickey, and J. J. Adams, "A compound frequency-and polarization-reconfigurable crossed dipole using multidirectional spreading of liquid metal," *IEEE Antennas Wireless Propag. Lett.*, vol. 16, pp. 79–82, 2017.

[14] C. Wang, J. C. Yeo, H. Chu, C. T. Lim, and Y.-X. Guo, "Design of a reconfigurable patch antenna using the movement of liquid metal," *IEEE Antennas Wireless Propag. Lett.*, vol. 17, no. 6, pp. 974–977, Jun. 2018.

[15] A. Arbelaez-Nieto, J.-L. Olvera-Cervantes, C. E. Saavedra, and A. Corona-Chavez, "Balanced liquid metal reconfigurable microstrip filter," *J. Electromagn. Waves Appl.*, vol. 31, no. 14, pp. 1453–1466, 2017.

[16] G. Mumcu, A. Dey, and T. Palomo, "Frequency-agile bandpass filters using liquid metal tunable broadside coupled split ring resonators," *IEEE Microw. Wireless Compon. Lett.*, vol. 23, no. 4, pp. 187–189, Apr. 2013.

[17] C. B. Eaker and M. D. Dickey, "Liquid metal actuation by electrical control of interfacial tension," *Appl. Phys. Rev.*, vol. 3, no. 3, Aug. 2016, Art. no. 031103.

[18] A. V. Diebold *et al.*, "Electrowetting-actuated liquid metal for RF applications," *J. Micromech. Microeng.*, vol. 27, no. 2, 2017, Art. no. 025010.

[19] W. Su, B. Cook, M. Tentzeris, C. Mariotti, and L. Roselli, "A novel inkjet-printed microfluidic tunable coplanar patch antenna," in *Proc. IEEE Antennas Propag. Soc. Int. Symp. (APSURSI)*, Jul. 2014, pp. 858–859.

[20] M. D. Brown and C. E. Saavedra, "Tunable branchline coupler using microfluidic channels," *IEEE Microw. Wireless Comp. Lett.*, vol. 20, no. 3, pp. 207–209, Mar. 2019.

[21] G. Dufour, N. Tiercelin, W. T. Khan, P. Coquet, P. Pernod, and J. Papapolymerou, "Large frequency tuning of a millimeter-wave antenna using dielectric liquids in integrated micro-channels," in *IEEE MTT-S Int. Microw. Symp. Dig.*, May 2015, pp. 1–4.

[22] S. Wang, L. Zhu, J. Wang, and W. Wu, "Low-loss transformer oil for application in frequency-reconfigurable lp/cp patch antennas," in *Proc. Int. Conf. Microw. Millim. Wave Technol. (ICMMT)*, May 2018, pp. 1–3.

[23] S. Wang, Z. Hu, W. Wu, and Z. Shen, "A low-profile frequency and polarization reconfigurable circularly polarized water antenna for satellite navigation," in *2016 IEEE Int. Symp. Antennas Propag. (APSURSI)*, Jun./Jul. 2016, pp. 1507–1508.

[24] S. S. Alja'afreh, Y. Huang, and L. Xing, "A compact dual-feed water-based diversity antenna," in *Proc. Loughborough Antennas Propag. Conf. (LAPC)*, Nov. 2013, pp. 182–185.

[25] J. Sun and K.-M. Luk, "Design of a 2×2 water dielectric patch antenna array for Wi-Fi application," in *Proc. IEEE Asia–Pacific Conf. Antennas Propag. (APCAP)*, Jun./Jul. 2015, pp. 237–238.

[26] Y.-H. Qian and Q.-X. Chu, "A polarization-reconfigurable water-loaded microstrip antenna," *IEEE Antennas Wireless Propag. Lett.*, vol. 16, pp. 2179–2182, 2017.

[27] I. Goode and C. E. Saavedra, “A four element phased patch antenna array using fluidic phase shifter,” in *Proc. URSI GASS*, Montreal, QC, Canada, Aug. 2017, pp. 1–2.
[28] J.-J. Liang, G.-L. Huang, K.-W. Qian, S.-L. Zhang, and T. Yuan, “An azimuth-pattern reconfigurable antenna based on water grating reflector,” *IEEE Access*, vol. 6, pp. 34804–34811, 2018.
[29] D.-C. Son *et al.*, “Design of a hemispherical reconfigurable frequency selective surface using water channels,” *IEEE Access*, vol. 6, pp. 61445–61451, 2018.
[30] Z. Hu, S. Wang, Z. Shen, and W. Wu, “Broadband polarization-reconfigurable water spiral antenna of low profile,” *IEEE Antennas Wireless Propag. Lett.*, vol. 16, pp. 1377–1380, 2017.
[31] Y.-H. Qian and Q.-X. Chu, “A pattern-reconfigurable water-loaded MIMO antenna,” *Microw. Opt. Technol. Lett.*, vol. 59, no. 7, pp. 1608–1613, Jul. 2017.
[32] A. Singh and C. E. Saavedra, “A frequency-reconfigurable water-loaded planar monopole antenna,” in *Proc. Int. Symp. Antenna Technol. Appl. Electromag. (ANTEM)*, Aug. 2018, pp. 1–4.
[33] A. Singh, I. Goode, and C. E. Saavedra, “A multistate frequency reconfigurable monopole antenna using fluidic channels,” *IEEE Antennas Wireless Propag. Lett.*, vol. 18, no. 5, pp. 856–860, May 2019, doi: 10.1109/LAWP.2019.2903781.
[34] D. M. Pozar, *Microwave Engineering*. Hoboken, NJ, USA: Wiley, 1998.
[35] D. G. Long and F. T. Ulaby, *Microwave Radar and Radiometric Remote Sensing*, vol. 4. Ann Arbor, MI, USA: University Michigan Press, 2014.
[36] D. Sarkar, A. Singh, K. Saurav, and K. V. Srivastava, “Four-element quad-band multiple-input–multiple-output antenna employing split-ring resonator and inter-digital capacitor,” *IET Microw., Antennas Propag.*, vol. 9, no. 13, pp. 1453–1460, 2015.
[37] A. Dey and G. Mumcu, “Microfluidically controlled frequency-tunable monopole antenna for high-power applications,” *IEEE Antennas Wireless Propag. Lett.*, vol. 15, pp. 226–229, 2016.

**Aditya Singh** received the B.E. degree in electronics and telecommunication engineering from the Jabalpur Engineering College, Jabalpur, India, in 2012, and the M.Tech. degree in R.F. and microwave from IIT Kanpur, Kanpur, India, in 2014. He is currently pursuing the Ph.D. degree with the Department of Electrical and Computer Engineering, Queen’s University, Kingston, ON, Canada.

From 2014 to 2017, he was an Edison Engineer with General Electric (GE) Transportation, Bengaluru, India, where he was involved in control system design for GE locomotives. His current research interests include antenna design for 5G systems, massive multiple-input–multiple-output antenna systems, and reconfigurable antenna design employing microfluidics.

Mr. Singh was a recipient of the Ontario Trillium Scholarship (OTS) from the Government of Ontario, Canada.

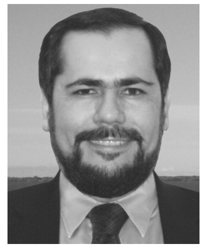

**Carlos E. Saavedra** (S’92–M’98–SM’05) received the B.Sc. degree from the University of Virginia, Charlottesville, VA, USA, and the M.Sc. and Ph.D. degrees from Cornell University, Ithaca, NY, USA, all in electrical engineering.

From 1998 to 2000, he was a Senior Engineer with Millitech Corporation, Northampton, MA, USA. In 2000, he joined the Department of Electrical and Computer Engineering, Queen’s University, Kingston, ON, USA, where he is currently a Professor. He has served as the ECE Chair of Graduate Studies with Queen’s University from 2007 to 2010. During sabbatical leaves, he held visiting appointments at the University of Navarra, Pamplona, Spain, the Universidade Federal do Rio Grande do Sul, Porto Alegre, Brazil, and the University of Twente, Enschede, The Netherlands.

Prof. Saavedra is also a Steering Committee Member of the IEEE International Microwave Symposium (Montreal) and a Technical Program Committee Member of the IEEE MTT-S International microwave symposium (IMS), the IEEE RFIC Symposium, the IEEE NEWCAS Conference, the Asia–Pacific Microwave Conference, and the IEEE MTT-S Latin America Microwave Conference (LAMC). He was a prior recipient of the NSERC Discovery Accelerator Award. He coauthored/supervised the Best Student Paper at the 2009 IEEE SiRF Conference. He was a three-time recipient of the ECE Undergraduate Teaching Award at Queen’s University. He is also the Chair of the IEEE MTT-S Technical Coordinating Committee on Signal Generation and Frequency Conversion and the IEEE AP/MTT Kingston Joint Chapter and the Vice-Chair of the IEEE Kingston Section. He is also the TPC Track Chair for IEEE MTT-S International Microwave and RF Conference (IMaRC) and IEEE Latin American Symposium on Circuits and Systems (LASCAS). He is also the former Co-Chair of the Natural Sciences and Engineering Research Council of Canada (NSERC) Discovery Grant Evaluation Group for Electrical and Computer Engineering. He is also a Co-PI of the Platform for Advanced Design Leading to Manufacturing in Micro-Nano Technologies, a multimillion-dollar national infrastructure project from 2015 to 2020, funded by the Canada Foundation for Innovation (CFI) and Provincial Governments. He has served on grant review panels at the National Science Foundation (USA) and as an External Reviewer for the Netherlands Organisation for Scientific Research. He is also a former Associate Editor of the IEEE TRANSACTIONS ON MICROWAVE THEORY AND TECHNIQUES and a Guest Editor of the *IEEE Microwave Magazine*. He is also a registered Professional Engineer (P.Eng.) in the Province of Ontario, Canada.